

# Clamped-Clamped Microbeam Resonators of Enhanced Higher Order-Modes Response and Wide Bandwidth

Nizar R. Jaber, Abdallah Ramini, Mohammad I. Younis  
Physical Science and Engineering Division  
King Abdullah University of Science and Technology (KAUST)  
Thuwal 23955-6900, Saudi Arabia

e-mail: [Nizar.jaber@kaust.edu.sa](mailto:Nizar.jaber@kaust.edu.sa), [Abdallah.ramini@kaust.edu.sa](mailto:Abdallah.ramini@kaust.edu.sa), [Mohammad.younis@kaust.edu.sa](mailto:Mohammad.younis@kaust.edu.sa)

**Abstract**—In this study, we present an experimental investigation of electrically actuated clamped-clamped microbeam resonators. The objective is to excite the higher order modes of the microbeams using partial electrodes with shapes that induce strong excitation of the mode of interest. The devices are fabricated using polyimide as a structural layer coated with Nickel from top and Chrome and Gold layers from bottom. Using a high frequency laser Doppler vibrometer, the first three resonance frequencies are revealed via white noise signals. Then, we studied the nonlinear dynamics of the microbeams near these resonance frequencies by applying forward frequency sweep with different electro dynamical loading conditions. The reported results prove the ability to excite higher order modes effectively using partial electrodes. Using a half electrode, the second mode is excited with high amplitude compared with almost zero response using the full electrode. Also, we present an experimental study of an electrically actuated clamped-clamped microbeam under a two-source harmonic excitation. The first frequency is swept around the first and second mode of vibration where the second one is fixed. The excitation of additive and subtractive type resonances is highlighted. In addition, we show that by properly tuning the frequency and the amplitude of the excitation force, the frequency bandwidth of the resonator is increased. Such micro-resonator is shown to be promising in gas and mass detection applications.

**Keywords**—*Electrostatic; multifrequency; resonator; higher order modes.*

## I. INTRODUCTION

Micro-electromechanical systems (MEMS) are devices and technologies that have been evolved from the microelectronics industry. Researchers have investigated different ways to create MEMS devices using microelectronic fabrication method. MEMS devices have attractive features, such as the smaller size, the ability to work in harsh environment, and power efficiency [1][2]. In particular, MEMS resonators composed mainly of microbeams are the main building block of many MEMS sensors and actuators that are used in variety of applications, such as toxic gas sensors [3], mass and biological sensors [4-7], temperature sensors [8], force and acceleration sensors [9], and earthquake detectors [10]. MEMS resonators are excited using different types of forces, such as piezoelectric [11][12], thermal [13], and electrostatic [10][14].

Electrostatic and electrodynamic excitations are the most commonly used method because of simplicity and availability [14][15]. The nonlinear dynamics of electrostatically actuated resonator is studied intensively and thoroughly in [14- 20].

MEMS resonators excited near their higher order modes have been proposed for mass and gas detection. Exciting the resonators near their higher order modes improve the sensitivity and the quality factor of the mass sensor. In [12], the sensitivity  $S_n$  and the quality factor  $Q_n$  of a resonant cantilever is defined as

$$S_n = \frac{\omega'_n - \omega_n}{m} \approx \frac{-\omega_n}{2m_{eff}} \quad (1)$$

$$Q_n = 3\pi b h \omega_n (256\mu)^{-1} \quad (2)$$

where  $m$  is the cantilever mass,  $m_{eff}$  is the  $n^{th}$  mode effective mass of the cantilever,  $\omega_n$  is the resonance frequency of the cantilever,  $\omega'_n$  is the final resonance frequency after detecting a mass,  $b$  is the beam width,  $h$  is the thickness and  $\mu$  is the air viscosity. As noticed from (1) and (2) the sensitivity and the quality factor are directly proportional to the excited mode number. High quality factor implies a sharper and stable resonance peak. This can be achieved through increasing  $\omega_n$  and decreasing  $m_{eff}$ ; both are achieved through high-order mode excitations.

There is an increasing demand to develop resonant sensors with large frequency band and low power consumptions [3][4][21]. An efficient approach to improve the vibration of resonator and increase the frequency band is to use parametric excitation [16], secondary resonance [21], slightly buckled resonators [22] and multi frequency excitation [23]. A device with tunable resonant frequency for energy harvesting application is designed and tested in [24]. They increased the resonant frequency band up to  $\pm 20\%$  of the original resonant frequency using a permanent magnet. The effect of the double potential well systems on the resonant frequency band and their application in energy harvesting application is reviewed in [25]. Also, Cho et al. [26] they designed and characterized a carbon nanotube based nano-resonator for mass detection application, they proved that the resonator bandwidth is directly proportional to the forcing amplitude.

Recent research highlighted the interesting dynamics of mixed frequency excitation and their applications as sensors and actuators. Mixed frequency excitation of a micro mirror is studied intensively by Ilyas et al. [23]. They proposed mixed frequency excitation as way to improve bandwidth in resonators. Parametrically and harmonically excited a micro-ring gyroscope at two different frequencies is investigated in [27]. Using this method, they increased the signal to noise ratio and improved the performance of the gyroscope. In [28], they fabricated and characterized a device that harvests electromagnetic energy at the three different resonance frequencies of vibration. Moreover, the method of multi frequency excitation is implemented in [29] to perform mechanical logic operation where each frequency carries a different bit of information. In [30], the frequency mixing is exploited on the atomic force microscope (AFM) resonator to generate a high resolution imaging and extract the surface properties.

Our goal is to excite the higher modes by changing the lower electrode configuration such that it, to some extent, resembles the excited mode shape of the clamped-clamped micro-beam. As we can see in Figure 1, we use full electrode to excite first mode, half electrode to excite the second mode, and two-third electrodes spaced out along the beam length to excite the third mode.

Motivated by the interesting dynamic behavior of clamped-clamped microstructures excited by a multi-frequency electrical source and their wide range of applications, this paper also investigates the dynamics of the resonator shown in Figure 1 experimentally.

The paper is organized as follows. In Section 2, we present the fabrication process of the microbeams. The characterization setup and methodology used in extracting the data is presented in Section 3. In Section 4, we discuss and report the results to single frequency excitation near the first and second mode of vibration. The response to a multi frequency source is presented in Section 5. Summary of the

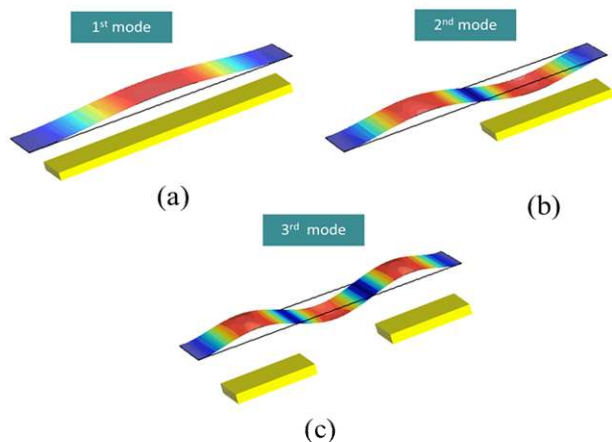


Figure 1. Clamped-clamped mode shapes with different lower electrode configuration. (a) Full electrode. (b) Half electrode. (c) Two-third electrode.

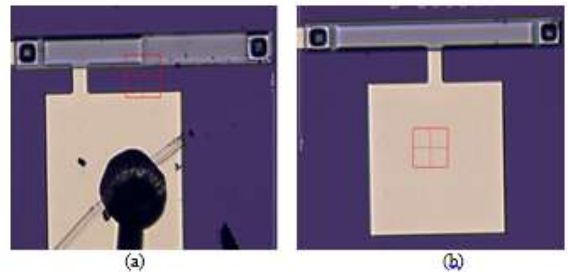


Figure 2. A top view picture of the fabricated microbeam and the actuation pad. (a) half lower electrode configuration. (b) full lower electrode configuration.

results and the potential applications is discussed in Section 6.

## II. FABRICATION

The clamped-clamped microstructure resonators are fabricated using the in-house process developed in [31][32]. The process consists of six physical layers shown in Figure 2 and set of rules that defines the allowed configuration and minimum feature size. The microstructure consists of a  $6\mu\text{m}$  polyimide structural layer coated with  $500\text{nm}$  nickel layer from top and  $50\text{nm}$  chrome  $250\text{nm}$  gold and  $50\text{nm}$  chrome from bottom. The chrome layer enhances the adhesion properties between gold and another materials. The Nickel layer protects the microbeam during the polyimide etch. The lower electrode is placed directly underneath the microstructure and composed of gold and chrome layers. It spans half of the microstructure length and provides the actuation force to the resonator. The two electrodes are separated with a  $2\mu\text{m}$  air gap. When the two electrodes are connected to an external excitation voltage, the resonator vibrates in the out-of-plane direction. Figure 3 shows a picture illustrating the various layers of the fabricated resonator. A  $500\mu\text{m}$   $\text{SiO}_2$  is thermally grown to provide insulation and enhance the adhesion properties between the lower electrode and the wafer.



Figure 3. Cross sectional view of the fabricated microbeam.



Figure 4. Experimental setup used for testing the MEMS device.

### III. CHARACTERIZATION

In this section, we describe the experimental set up used for testing the device and measuring the initial profile, gap thickness and the out-of-plane vibration. The experimental setup consists of a micro system analyzer (MSA) under which the microstructure is placed to measure the vibration, data acquisition cards and amplifiers to provide actuation signals of wide range of frequencies and amplitudes, a vacuum chamber equipped with ports to pass the actuation signal and measure the pressure. Also, the chamber is connected to a vacuum pump that reduces the pressure as low as  $4mTorr$ . The microbeam movement is measured using the laser-Doppler vibrometer. The laser beam was focused onto the microstructure using the microscope and the x-y positioning stage. The measurement is based on interferometry, where the laser beam is split into two beams: one focused on the moving structure and the other one focused on a reference target. The difference between the two beams in phase and distance traveled will be translated into displacement or velocity of the microstructure as a function of the frequency and time. The setup is shown in Figure 4.

#### A. Topography Characterization

The initial profile of the microstructure is revealed using an optical profilometer. After defining the vertical scanning range and exposure time, a 3-D map of the microbeam is generated, as depicted in Figure 5. The combined thickness of the microstructure and air gap is around  $9\mu m$ , which is slightly smaller from the design nominal value of  $9.35\mu m$ . Also, the microbeam total length is  $400\mu m$  and the

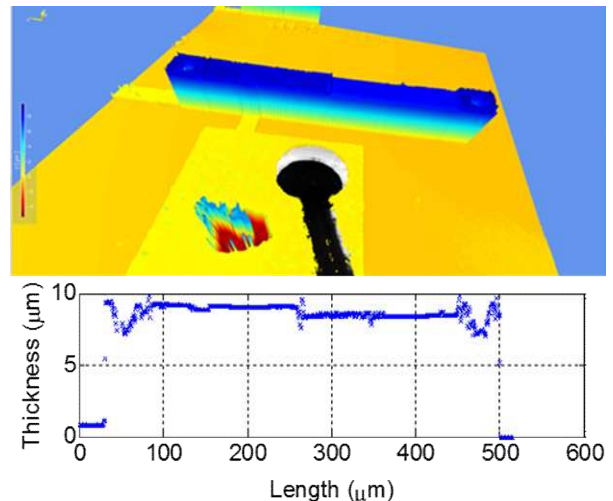


Figure 5. A 3-D map of the microbeam with half lower electrode configuration profile as seen from top.

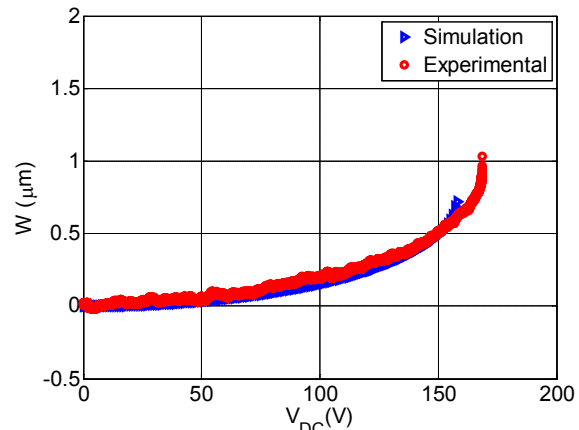


Figure 6. Static profile of the microbeam with half electrode actuation.

profile is fully straight without any curvature or curling.

#### B. Static Characterization

To characterize the device we initially biased the microbeam by a slow DC ramp voltage - generated using the data acquisition card - and measured the static deflection. The experimental result is reported in Figure 6. The deflection increases until it exhibits pull in at  $168V$  for a clamped beam with half electrode actuation.

#### C. Natural frequencies

We experimentally measured the first three natural frequencies by connecting the wire-bonded chip to the MSA function generator and applying a white noise signal. The MSA measures the microstructure vibration at the laser point position. Also, it has the capability to reveal the mode shape of the vibration.

The microstructure is excited with a white noise of  $V_{DC} = 30V$  and  $V_{AC} = 50V$ . The vibration at different points along the beam length is scanned to extract the vibration mode shapes and resonance frequencies. The acquired frequency response curve is shown in Figure 7 and it reveals the values of the first three natural

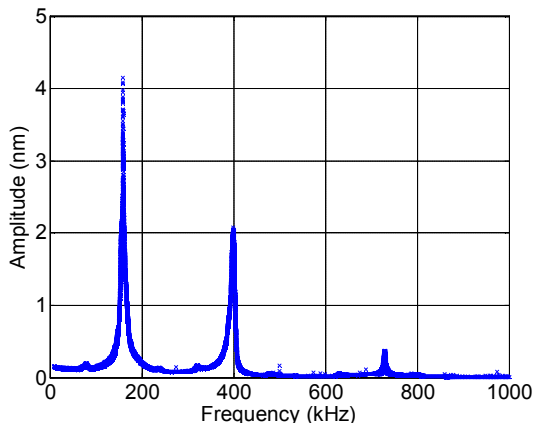


Figure 7. Frequency response curve of the microbeam with half electrode actuation to white noise actuation signal.  $V_{DC} = 30V$  and  $V_{AC} = 50V$  at  $4mTorr$  chamber pressure.

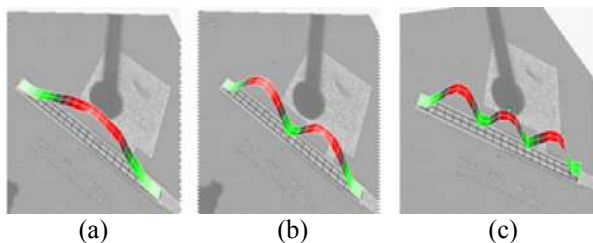


Figure 8. The vibrational mode shapes of the microbeam with half lower electrode configuration at (a)  $\omega_1 = 160kHz$ , (b)  $\omega_2 = 402kHz$  and  $\omega_3 = 738kHz$ .

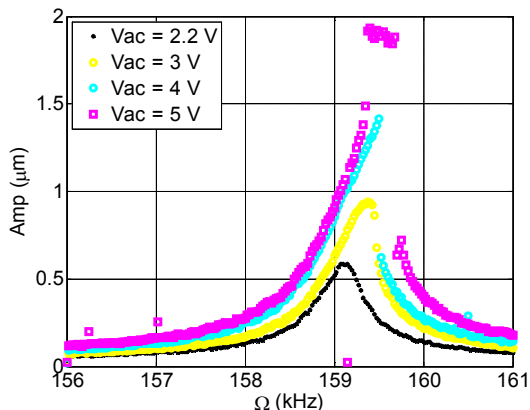


Figure 9. Frequency response curve for the microbeam near the first resonance with full lower electrode configuration.  $V_{DC} = 5V$ .

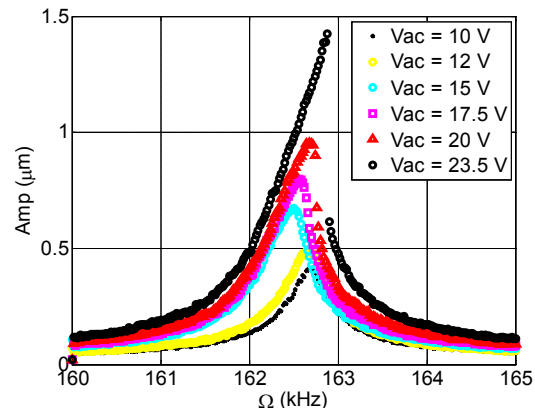


Figure 10. Frequency response curve for the microbeam near the first resonance with half lower electrode configuration.  $V_{DC} = 5V$ .

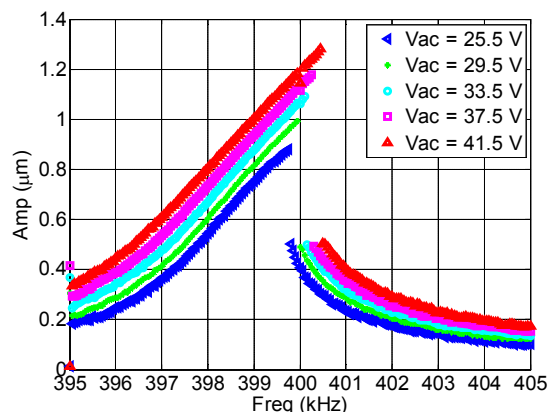


Figure 11. Frequency response curve for microbeam near the second resonance with half electrode actuation.  $V_{DC} = 30V$ .

frequencies  $\omega_1 = 160 kHz$ ,  $\omega_2 = 402 kHz$ , and  $\omega_3 = 738 kHz$ . The acquired vibration mode shapes of the test are reported in Figure 8. We notice at  $\omega_1$ , as shown in Figure 8(a) all points are vibrating whereas at  $\omega_2$  (see Figure 8(b)), the mid points are nodal points. Also, at  $\omega_3$  (see Figure 8(c)), there are two nodal points. These results match the clamped-clamped structure first, second and third vibration mode shapes.

#### IV. HIGHER ORDER MODES RESULTS

We experimentally investigate the nonlinear response of the microbeams near the first two resonance frequencies via frequency sweep tests. The micro-beams are excited using the data acquisition card and the vibration is detected using the MSA. The excitation signal is composed of an AC signal  $V_{AC}$  superimposed to a DC signal  $V_{DC}$ . The frequency response curve is generated by taking the steady state amplitude of the motion and focusing the laser at the mid-point of the microbeam for the first measurement and at quarter of the beam length for the second mode

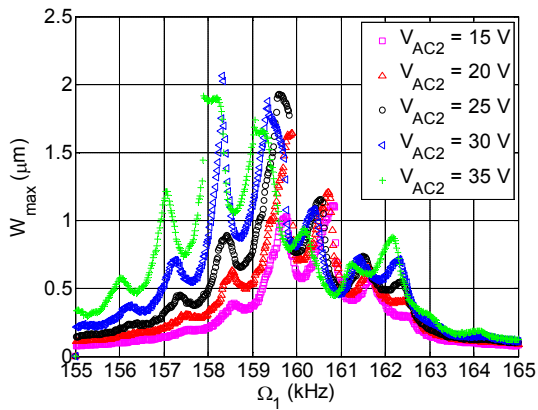


Figure 12. Frequency response curve for  $V_{DC} = 15V$ ,  $V_{AC1} = 5V$  and  $\Omega_2 = 1kHz$  near the first resonance.

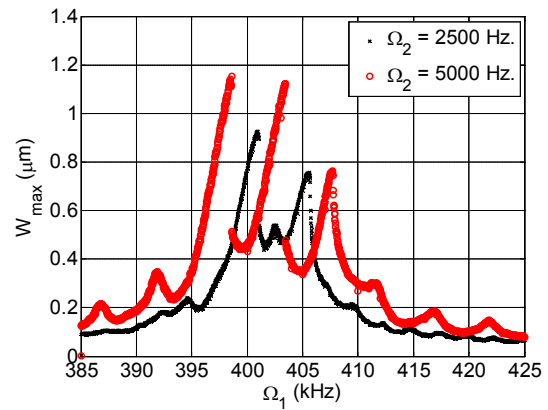


Figure 15. Frequency response curve for different values of  $\Omega_2$  at  $V_{DC} = 15V$ ,  $V_{AC1} = 20V$  and  $V_{AC2} = 70V$  near the second resonance.

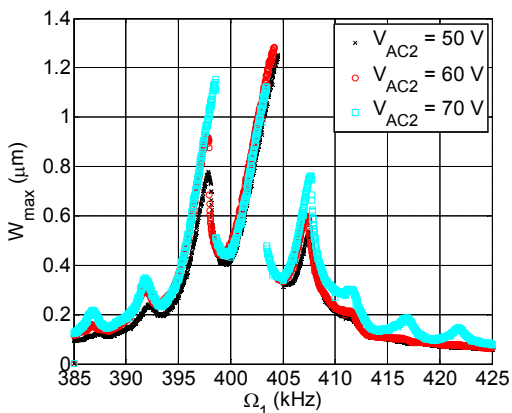


Figure 13. Frequency response curve for  $V_{DC} = 15V$ ,  $V_{AC1} = 20V$  and  $\Omega_2 = 5kHz$  near the second resonance.

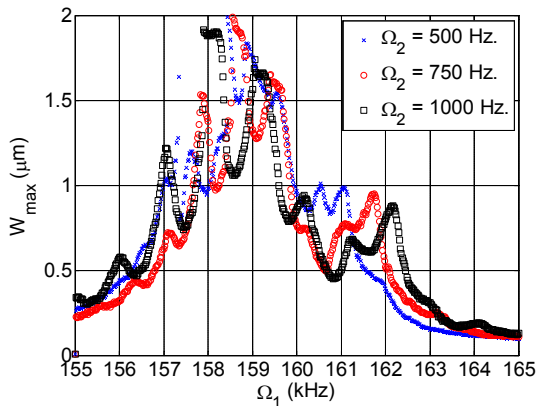


Figure 14. Frequency response curve for different values of  $\Omega_2$  at  $V_{DC} = 15V$ ,  $V_{AC1} = 5V$  and  $V_{AC2} = 35V$  near the first resonance.

measurement. In the following subsection, the frequency

response curves are reported for the different microbeams with full and half electrode actuation at different electrodynamical loadings and at  $4mTorr$  chamber pressure.

#### A. First Mode

Figures 9 and 10 show the variation of the frequency response curve as the AC voltage is increased for different lower electrode configuration near the first resonance. As expected, using the full electrode configuration we achieved higher amplitude near the first mode compared with the half electrode configurations under the same conditions of electro dynamical loading and vacuum chamber pressure. Also, a hardening effect is reported due to the cubic nonlinearities from mid-plane stretching.

#### B. Second Mode

Figure 11 shows the variation of the frequency response curve as the AC voltage is increased near the second mode resonance for the half electrode configuration. Using a half electrode, the second mode is excited with high amplitude compared with no response using the full electrode configuration. In addition, a hardening effect is reported due to the cubic nonlinearities.

### V. MULTIFREQUENCY EXCITATION RESULTS

We experimentally investigated the nonlinear response of the microbeams to a multi-frequency excitation near the first and second resonance frequencies. The microbeams are excited using the data acquisition card and the vibration is detected using the MSA. The excitation signal composed of two AC signals  $V_{AC1}$  and  $V_{AC2}$  of different frequencies  $\Omega_1$  and  $\Omega_2$  superimposed to a DC signal  $V_{DC}$ .

The generated frequency response curves near the first resonance are presented in Figure 12. Each curve shows the frequency response for different values of  $V_{AC2}$ . The results are obtained by sweeping the frequency  $\Omega_1$  of the first source  $V_{AC1}$  around the first mode and fixing the second

source  $V_{AC2}$  frequency  $\Omega_2$  at  $1\text{ kHz}$ . The swept source voltage  $V_{AC1}$  and the DC voltage are fixed at  $5\text{ V}$  and  $15\text{ V}$ , respectively. Figure 13 shows the result of sweeping the first source frequency  $V_{AC1}$  around the second mode while fixing the second source frequency  $V_{AC2}$  at  $5\text{ kHz}$ . The swept source voltage  $V_{AC1}$  and the DC voltage are fixed at  $20\text{ V}$  and  $15\text{ V}$ , respectively. The chamber pressure is fixed at  $4\text{ mTorr}$ . The curves highlight the effect of  $V_{AC2}$  on the combination resonances where new resonance peaks appear at frequencies of additive type at  $(\Omega_1 + \Omega_2)$ ,  $(\Omega_1 + 2\Omega_2)$ ,  $(\Omega_1 + 3\Omega_2)$  and subtractive type at  $(\Omega_1 - \Omega_2)$ ,  $(\Omega_1 - 2\Omega_2)$ ,  $(\Omega_1 - 3\Omega_2)$ . These resonances arise due to the cubic nonlinearity coming from the midplane stretching effect and the electrostatic force. Also, as  $V_{AC2}$  increases the response curves tilt towards the lower frequency values (softening). Figure 14 and 15 show the result for different values of  $\Omega_2$  under the same electrodynamic loading condition near the first and second resonance frequencies, respectively. As  $\Omega_2$  decreases, a continuous band of high amplitude is formed.

## VI. CONCLUSIONS

In this paper, we investigated the dynamics of clamped-clamped microbeam with full and half lower electrode configuration. These microbeams are electrically actuated by an AC source with variable frequency superimposed to a DC voltage. We proved the ability to excite the second mode resonance by using a half electrode configuration. Also, a hardening behavior is reported due to the cubic nonlinearities among all the excited modes due to the dominating effect of mid-plane stretching. In addition, we investigated the dynamics of clamped-clamped microbeams electrically actuated by two harmonic AC sources with different frequencies superimposed to a DC voltage. Moreover, the ability to excite the combination resonance of additive and subtractive type is proved.

This capability of exciting the higher order modes can have a promising application in MEMS-based mass, gas and humidity sensors. In addition, the ability to broaden the bandwidth of the resonator is shown by reducing the frequency of the fixed source. These capabilities of generating multiple peaks and a high response band with ability to control its amplitude and location can have a promising application in increasing the resonator band width, mechanical logic circuits, energy harvesting and mass sensing.

## REFERENCES

- [1] B. Kim, et al., "Using MEMS to build the device and the package," in Solid-State Sensors, Actuators and Microsystems Conference, 2007. TRANSDUCERS 2007. International, 2007, pp. 331-334.
- [2] B. Kim, et al., "CMOS Compatible Wafer-Scale Encapsulation MEMS Resonators," in ASME 2007 InterPACK Conference collocated with the ASME/JSME 2007 Thermal Engineering Heat Transfer Summer Conference, 2007, pp. 499-504.
- [3] S. Subhashini and A. Vimala Juliet, "Toxic gas sensor using resonant frequency variation in micro-cantilever," in Sustainable Utilization and Development in Engineering and Technology (STUDENT), 2012 IEEE Conference on, 2012, pp. 87-91.
- [4] S. Dohn, R. Sandberg, W. Svendsen, and A. Boisen, "Enhanced functionality of cantilever based mass sensors using higher modes," Applied Physics Letters, vol. 86, pp. 233501, 2005.
- [5] E. Gil-Santos, et al., "Nanomechanical mass sensing and stiffness spectrometry based on two-dimensional vibrations of resonant nanowires," Nature nanotechnology, vol. 5, pp. 641-645, 2010.
- [6] M. Hanay, et al., "Single-protein nanomechanical mass spectrometry in real time," Nature nanotechnology, vol. 7, pp. 602-608, 2012.
- [7] T. P. Burg, et al., "Vacuum-packaged suspended microchannel resonant mass sensor for biomolecular detection," Microelectromechanical Systems, Journal of, vol. 15, pp. 1466-1476, 2006.
- [8] W.-T. Hsu, J. R. Clark, and C. T.-C. Nguyen, "A resonant temperature sensor based on electrical spring softening," in Tech. Dig., 11th Int. Conf. on Solid-State Sensors Actuators (Transducers' 01), Munich, Germany, 2001, pp. 1484-1487.
- [9] H. C. Kim, S. Seok, I. Kim, S.-D. Choi, and K. Chun, "Inertial-grade out-of-plane and in-plane differential resonant silicon accelerometers (DRXLs)," in Solid-State Sensors, Actuators and Microsystems, 2005. Digest of Technical Papers. TRANSDUCERS'05. The 13th International Conference on, 2005, pp. 172-175.
- [10] A. Ramini, K. Masri, and M. I. Younis, "Electrostatically actuated resonant switches for earthquake detection," in Mechatronics and its Applications (ISMA), 2013 9th International Symposium on, 2013, pp. 1-7.
- [11] B. Piekarski, et al., "Fabrication of suspended piezoelectric microresonators," Integrated Ferroelectrics, vol. 24, pp. 147-154, 1999.
- [12] D. Jin, et al., "High-mode resonant piezoresistive cantilever sensors for tens-femtogram resolvable mass sensing in air," Journal of Micromechanics and Microengineering, vol. 16, pp. 1017, 2006.
- [13] G. Rinaldi, M. Packirisamy, and I. Stiharu, "Quantitative boundary support characterization for cantilever MEMS," Sensors, vol. 7, pp. 2062-2079, 2007.
- [14] M. I. Younis, MEMS Linear and Nonlinear Statics and Dynamics: Memes Linear and Nonlinear Statics and Dynamics vol. 20: Springer Science & Business Media, 2011.
- [15] J. F. Rhoads, S. W. Shaw, and K. L. Turner, "Nonlinear dynamics and its applications in micro- and nanoresonators," Journal of Dynamic Systems, Measurement, and Control, vol. 132, pp. 034001, 2010.
- [16] R. Kalyanaraman, G. Rinaldi, M. Packirisamy, and R. Bhat, "Equivalent area nonlinear static and dynamic analysis of electrostatically actuated microstructures," Microsystem technologies, vol. 19, pp. 61-70, 2013.
- [17] F. M. Alsaleem, M. I. Younis, and H. M. Ouakad, "On the nonlinear resonances and dynamic pull-in of electrostatically actuated resonators," Journal of Micromechanics and Microengineering, vol. 19, p. 045013, 2009.
- [18] J. F. Rhoads, V. Kumar, S. W. Shaw, and K. L. Turner, "The nonlinear dynamics of electromagnetically actuated microbeam resonators with purely parametric excitations," International Journal of Non-Linear Mechanics, vol. 55, pp. 79-89, 2013.
- [19] M. Younis and A. Nayfeh, "A study of the nonlinear response of a resonant microbeam to an electric actuation," Nonlinear Dynamics, vol. 31, pp. 91-117, 2003.
- [20] M. Younis, "Multi-mode excitation of a clamped-clamped microbeam resonator," Nonlinear Dynamics, vol. 80, pp. 1531-1541, 2015/05/01 2015.
- [21] A. H. Nayfeh and M. I. Younis, "Dynamics of MEMS resonators under superharmonic and subharmonic excitations," Journal of Micromechanics and Microengineering, vol. 15, p. 1840, 2005.
- [22] M. Bagheri, M. Poot, M. Li, W. P. Pernice, and H. X. Tang, "Dynamic manipulation of nanomechanical resonators in the high-amplitude regime and non-volatile mechanical memory operation," Nature nanotechnology, vol. 6, pp. 726-732, 2011.
- [23] S. Ilyas, A. Ramini, A. Arevalo, and M. I. Younis, "An Experimental and Theoretical Investigation of a Micromirror Under Mixed-Frequency Excitation." (DOI:10.1109/JMEMS.2014.2386285).

- [24] V. R. Challa, M. Prasad, Y. Shi, and F. T. Fisher, "A vibration energy harvesting device with bidirectional resonance frequency tunability," *Smart Materials and Structures*, vol. 17, pp. 015035, 2008.
- [25] R. Harne and K. Wang, "A review of the recent research on vibration energy harvesting via bistable systems," *Smart Materials and Structures*, vol. 22, pp. 023001, 2013.
- [26] H. Cho, M.-F. Yu, A. F. Vakakis, L. A. Bergman, and D. M. McFarland, "Tunable, broadband nonlinear nanomechanical resonator," *Nano letters*, vol. 10, pp. 1793-1798, 2010.
- [27] B. Gallacher, J. Burdess, and K. Harish, "A control scheme for a MEMS electrostatic resonant gyroscope excited using combined parametric excitation and harmonic forcing," *Journal of Micromechanics and Microengineering*, vol. 16, pp. 320, 2006.
- [28] H. Liu, Y. Qian, and C. Lee, "A multi-frequency vibration-based MEMS electromagnetic energy harvesting device," *Sensors and Actuators A: Physical*, vol. 204, pp. 37-43, 2013.
- [29] I. Mahboob, E. Flurin, K. Nishiguchi, A. Fujiwara, and H. Yamaguchi, "Interconnect-free parallel logic circuits in a single mechanical resonator," *Nature communications*, vol. 2, pp. 198, 2011.
- [30] D. Forchheimer, D. Platz, E. A. Tholén, and D. B. Haviland, "Model-based extraction of material properties in multifrequency atomic force microscopy," *Physical Review B*, vol. 85, p. 195449, 2012.
- [31] L. Marnat, A. A. Carreno, D. Conchouso, M. G. Martinez, I. G. Foulds, and A. Shamim, "New Movable Plate for Efficient Millimeter Wave Vertical on-Chip Antenna," *IEEE Transactions on Antennas and Propagation*, vol. 61, pp. 1608-1615, 2013.
- [32] A. Alfadhel, A. A. Arevalo Carreno, I. G. Foulds, and J. Kosel, "Three-Axis Magnetic Field Induction Sensor Realized on Buckled Cantilever Plate," *Magnetics, IEEE Transactions on*, vol. 49, pp. 4144-4147, 2013.